Efficient dynamic simulations of charged dielectric colloids through a novel hybrid method

Zecheng Gan (iD), Ziwei Wang (iD), Shidong Jiang (iD), Zhenli Xu (iD), and Erik Luijten (iD)

View Online   Export Citation   CrossMark

The Journal of Chemical Physics

Submit Today

The Emerging Investigators Special Collection and Awards
Recognizing the excellent work of early career researchers!

AIP Publishing

Efficient dynamic simulations of charged dielectric colloids through a novel hybrid method

Zecheng Gan,[1,a] (iD) Ziwei Wang,[2,a] (iD) Shidong Jiang,[3] (iD) Zhenli Xu,[4] (iD) and Erik Luijten[5,b] (iD)

AFFILIATIONS

[1] Department of Mathematics, University of Michigan, Ann Arbor, Michigan 48109, USA
[2] Applied Physics Graduate Program, Northwestern University, Evanston, Illinois 60208, USA
[3] Department of Mathematical Sciences, New Jersey Institute of Technology, Newark, New Jersey 07102, USA
[4] School of Mathematical Sciences, Institute of Natural Sciences, and MoE Key Lab of Scientific
  and Engineering Computing, Shanghai Jiao Tong University, Shanghai 200240, China
[5] Departments of Materials Science and Engineering, Engineering Sciences and Applied Mathematics, Chemistry,
  and Physics and Astronomy, Northwestern University, Evanston, Illinois 60208, USA

[a] **Contributions:** Z. Gan and Z. Wang contributed equally to this work.
[b] **Electronic mail:** luijten@northwestern.edu

ABSTRACT

Modern particle-based simulations increasingly incorporate polarization charges arising from spatially nonuniform permittivity. For complex dielectric geometries, calculation of these induced many-body effects typically requires numerical solvers based upon boundary-element methods, which very significantly increase the required computational effort. For the special case of dielectric spheres, such as colloids or nanoparticles, we recently proposed a semianalytical spectrally accurate hybrid method that combines the method of moments, the image-charge method, and the fast multipole method. The hybrid method is efficient and accurate even when dielectric spheres are closely packed. Here, we extend the method to the evaluation of direct and induced electrostatic forces and demonstrate how this can be incorporated in molecular dynamics simulations. The choice of the relevant numerical parameters for molecular dynamics simulations is discussed in detail, as well as comparisons to the boundary-element method. As a concrete example, we examine the challenging case of binary crystal structures composed of close-packed dielectric colloidal spheres.

Published under license by AIP Publishing. https://doi.org/10.1063/1.5110628

I. INTRODUCTION

Electrostatic interactions are ubiquitous in nature and arise in many areas of science and engineering.[1–3] Whereas the long-range nature of these interactions makes their computational treatment already costly, the problem is compounded in systems with spatially nonuniform permittivity. Materials that differ in dielectric constant respond differently to electric fields, a property that—for systems with piecewise uniform permittivity—can be described in terms of an induced surface charge density distributed on the dielectric interfaces. This *polarization charge* contributes to the electric field and hence must be solved self-consistently.[4,5] Due to the

computational effort involved, this contribution is often ignored, but various studies have demonstrated that this approximation can have profound consequences, as polarization can influence protein folding,[6] ion transport through pores[7] and nanochannels,[8] and nanoparticle aggregation and self-assembly.[9,10] As these many-body effects are often analytically intractable, computational methods constitute an important tool toward greater physical understanding of the underlying phenomena.

The practical computational challenge associated with investigating polarization effects arises from the difficulty in efficiently obtaining an accurate estimate for the polarization charge. Note that even if the polarization contribution can be accurately resolved,

the calculation usually becomes very demanding in the context of molecular dynamics (MD) or Monte Carlo (MC) simulations. The internal energy or forces need to be evaluated at each time step, and typically millions of time steps are required to obtain sufficient data for accurate ensemble averages, even after reaching thermodynamic equilibrium.

To overcome this computational challenge, various numerical methods have been proposed.[11–27] Electrostatic solvers using finite-difference and finite-element methods[1,16] are less efficient for practical MD/MC simulations since (i) they require discretizing the entire three-dimensional (3D) space and (ii) special treatment is needed to accurately model sharp dielectric interfaces and point charges. In the latter case, boundary element methods (BEMs)[11–14,17,19,22–24,26] offer an alternative. The BEM reduces the 3D electrostatic Poisson equation to a boundary integral equation, thus only requiring the discretization of two-dimensional dielectric interfaces. The first MD simulation for *mobile* dielectric objects was carried out using this approach, studying a system of 100 dielectric spheres.[9] Yet, the BEM remains highly time consuming, in particular, for dielectric interfaces that are closely spaced. This situation typically arises in self-assembly processes of densely packed structures, where a large amount of boundary elements are required to resolve the numerical singularity due to nearly touching interfaces.

Instead of considering dielectric interfaces with arbitrary shape, the numerical difficulties can be reduced if we start with models that are comprised of simple geometric shapes yet still capture the essential physics. Naturally, the simplest case is based on the primitive model, i.e., an ensemble of dielectric spheres with central charges, immersed in a solvent modeled implicitly as a dielectric continuum. For such systems of charged dielectric spheres, alternative approaches can be employed to solve the electrostatic potential, e.g., the Method of Moments (MoM),[28–32] the Image Charge Method (ICM),[33–35] and the perturbative many-body expansion method.[36,37] These methods are developed by taking advantage of the spherical geometry and based on analytical forms, thus avoiding the need to discretize the dielectric boundaries into elements. The MoM scales as $\mathcal{O}(N)$ if accelerated using the Fast Multipole Method (FMM),[38–40] where N is the total number of spheres. However, it suffers from slow convergence if spheres are close. The ICM is both accurate and efficient if there are only one or two spheres, but as the number of spheres grows, the ICM computational cost increases as a power law [typically $\mathcal{O}(N^3)$, see Ref. 41] due to the repeated image reflection between spheres. Finally, the perturbative many-body expansion method is also an analytical method tailored for charged dielectric sphere systems, again with computational complexity that scales as $\mathcal{O}(N^m)$ if the expansion is truncated at the level of m-body interactions. As the expansion converges more slowly if spheres get closer, this approach (just like the ICM) becomes costly for systems of closely spaced objects. An alternative method in this category is the hybrid method we developed in Ref. 42, an efficient and spectrally accurate semianalytical approach for solving the electrostatics in systems of multiple dielectric spheres. For this approach, we first extended the ICM to analytically account for the effect of multipoles in the 3D dielectric case. We then combined the MoM, the ICM, and the FMM to obtain an accurate and well-conditioned numerical method that requires a nearly optimal number of unknowns with optimal $\mathcal{O}(N)$ computational complexity. It is worth noting that

the hybrid method works well even for compact configurations of spheres since the most singular part of the problem is removed by the ICM.

It is the purpose of the present work to extend the hybrid method of Ref. 42 for practical use in MD simulations. Specifically, we address the key issues for the implementation, including a detailed derivation of the expressions for the electrostatic energy, surface charge density, and forces on individual dielectric spheres. We also present numerical tests to determine the dependence of the accuracy and efficiency of the hybrid method on various numerical parameters and perform a comparison of our method with the BEM. By matter of illustration, we carry out efficient MD simulations using the hybrid method for a representative binary mixture of dielectric spheres. We conclude with a discussion of the possible extensions of our method to other systems, periodic boundary conditions, and MC simulations.

II. MODEL DEFINITION

We consider an ensemble of N dielectric spheres, in which sphere i ($i = 1, \ldots, N$) is centered at $\mathbf{o}_i$, has a radius a_i and a dielectric constant ε_i, and carries a central charge Q_i. The spheres do not overlap and are embedded in a continuum background solvent with dielectric constant ε_s. The internal dielectric constants ε_i are generally different from ε_s, resulting in polarization contributions to the electrostatic potential that need to be resolved.

We start by seeking the expression for the electrostatic energy. First, for any given free charge density $\rho_f(\mathbf{r})$ that generates a potential field $\Phi(\mathbf{r})$ and is embedded in a dielectric medium, the electrostatic energy U can be written as[4]

$$U = \frac{1}{2} \int \rho_f(\mathbf{r}) \Phi(\mathbf{r}) d\mathbf{r}. \tag{1}$$

In our model, the free charge density originates from the N point charges at the centers of the dielectric spheres, i.e.,

$$\rho_f(\mathbf{r}) = \sum_{i=1}^{N} Q_i \delta(\mathbf{r} - \mathbf{o}_i), \tag{2}$$

where $\delta(\cdot)$ is the Dirac delta function. Moreover, the electrostatic potential $\Phi(\mathbf{r})$ satisfies the Poisson equation,

$$-\nabla \cdot [\varepsilon(\mathbf{r}) \nabla \Phi(\mathbf{r})] = \rho_f(\mathbf{r}), \tag{3}$$

where

$$\varepsilon(\mathbf{r}) = \begin{cases} \varepsilon_i & \text{if } \mathbf{r} \text{ inside sphere } i, \\ \varepsilon_s & \text{if } \mathbf{r} \text{ in the exterior region,} \end{cases} \tag{4}$$

and on each spherical interface S_i ($i = 1, \ldots, N$), the electric potential $\Phi(\mathbf{r})$ has to satisfy the standard dielectric interface conditions,

$$\Phi(\mathbf{r}^-) = \Phi(\mathbf{r}^+), \qquad \mathbf{r} \in S_i, \tag{5}$$

$$\varepsilon_i \frac{\partial \Phi(\mathbf{r})}{\partial \mathbf{n}} \bigg|_{\mathbf{r}=\mathbf{r}^-} = \varepsilon_s \frac{\partial \Phi(\mathbf{r})}{\partial \mathbf{n}} \bigg|_{\mathbf{r}=\mathbf{r}^+}, \qquad \mathbf{r} \in \mathcal{S}_i, \tag{6}$$

where $\mathbf{r}^-$ and $\mathbf{r}^+$ refer to the limits approaching the interface from the inside and outside, respectively, and $\mathbf{n}$ is the surface outward unit normal vector at $\mathbf{r}$. In addition, we impose the vanishing far-field boundary condition, i.e., $\Phi(\mathbf{r}) \to 0$ as $|\mathbf{r}| \to \infty$. Once $\Phi(\mathbf{r})$ has

been obtained, the electrostatic energy can be calculated and the electrostatic forces can be obtained through differentiation.

It is worth noting that an alternative way to solve for the electrostatic potential $\Phi(\mathbf{r})$ is via the bound charge density $\rho_b(\mathbf{r})$, which satisfies

$$\rho_b(\mathbf{r}) = -\nabla \cdot \mathbf{P}(\mathbf{r}). \tag{7}$$

Assuming a linear polarization field $\mathbf{P}(\mathbf{r}) = [\varepsilon(\mathbf{r}) - 1]\mathbf{E}(\mathbf{r})$ and substituting the electric field $\mathbf{E}(\mathbf{r}) = -\nabla\Phi(\mathbf{r})$, one obtains

$$\rho_b(\mathbf{r}) = \nabla \cdot \{[\varepsilon(\mathbf{r}) - 1]\nabla\Phi(\mathbf{r})\}. \tag{8}$$

Combining this expression with Eq. (3), one obtains the well-known result[43]

$$-\nabla^2\Phi(\mathbf{r}) = \rho_f(\mathbf{r}) + \rho_b(\mathbf{r}). \tag{9}$$

This is a Poisson equation with a constant coefficient so that the solution $\Phi(\mathbf{r})$ can be simply represented as the standard Coulomb potential due to both the free and the bound charge density,

$$\Phi(\mathbf{r}) = \int \frac{\rho_f(\mathbf{r}') + \rho_b(\mathbf{r}')}{4\pi|\mathbf{r} - \mathbf{r}'|} d\mathbf{r}'. \tag{10}$$

Substitution of Eq. (10) into Eq. (1) allows the electrostatic energy to be expressed as

$$U = \frac{1}{8\pi} \iint \rho_f(\mathbf{r}) \frac{[\rho_f(\mathbf{r}') + \rho_b(\mathbf{r}')]}{|\mathbf{r} - \mathbf{r}'|} d\mathbf{r}' d\mathbf{r}. \tag{11}$$

The singularity at $\mathbf{r}' = \mathbf{r}$ due to the direct Coulomb interaction of point free charges should be discarded to render the integral finite. The remaining problem in Eq. (11) is that the bound charge density $\rho_b(\mathbf{r})$ is still unknown. For systems with arbitrarily shaped dielectric bodies, the BEM[26] can be employed to numerically obtain $\rho_b(\mathbf{r})$. For our system of dielectric spheres, the hybrid method framework[42] makes it possible to effectively represent the bound charge density $\rho_b(\mathbf{r})$ as a combination of multipole moments and image charges, as will be discussed in more detail in Sec. III.

III. REVIEW OF THE HYBRID METHOD

A. Overview

We now review the recently proposed hybrid method[42] for solving the electrostatic potential $\Phi(\mathbf{r})$ for the system described in Sec. II. Before presenting the detailed mathematical formulations, we first provide a brief overview and summarize the central idea of the hybrid method, which combines the numerical MoM and analytical ICM.

The MoM is a spectral method based on representing the solution of the Poisson equation in terms of spherical harmonics. It takes advantage of the spherical geometry of the interfaces and has been a popular method for determining the electrostatic potential and electric field in systems consisting of multiple dielectric spheres with various boundary conditions.[28–32] The advantages of the MoM are that—unlike BEMs and finite-element or finite-difference methods—it avoids discretization of space and that the

calculations involving spherical harmonics can be further accelerated via the FMM to achieve scaling that is linear in the number of spheres. However, the disadvantage of the MoM is that the rate of convergence of the spherical harmonic expansion is lowered dramatically when dielectric spheres are closely packed, making the MoM impractical for the study of systems of densely packed spheres.

Another classic methodology for the dielectric sphere system is the ICM. It is well known that the polarization potential generated by a point charge near a grounded or insulated conducting sphere can be treated as the potential generated by (fictitious) image charges.[4,33,34] For a point charge near a dielectric sphere, the solution is more complicated, but the polarization can again be expressed as a combination of image charges, namely, the sum of a point charge and a line charge with spatially varying charge density.[35] The advantage of the ICM is that it provides the exact potential even when charges are very close to the dielectric interface. However, the ICM becomes impractical for systems of multiple dielectric spheres since the total number of images increases as $\mathcal{O}(N^L)$, where N is the number of spheres and L is the level at which the image reflections are truncated (closely spaced spheres require $L \geq 3$, see Ref. 41).

The hybrid method was developed to exploit the advantages of both methods and avoid their shortcomings. For dielectric spheres that are well separated, the MoM can be used. If certain spheres in a configuration are close to each other, we modify the MoM by generating images only for nearly touching pairs of spheres. In Ref. 42, we demonstrated that this approach greatly accelerates the convergence of the MoM.

B. Method of moments

As the MoM relies on spherical harmonics, we first introduce relevant definitions and identities that are necessary for presenting the MoM to solve the electrostatic potential between charged dielectric spheres. First, the spherical harmonics are defined as

$$Y_n^m(\theta, \phi) = \sqrt{\frac{(n - |m|)!}{(n + |m|)!}} P_n^{|m|}(\cos\theta)e^{im\phi}, \tag{12}$$

for all integers $n \geq 0$ and $|m| \leq n$, where $P_n^{|m|}(\cdot)$ are the associated Legendre functions.[44] The general solution for the Laplace equation $\nabla^2\Phi(\mathbf{r}) = 0$ in spherical coordinates can be expressed using spherical harmonics as[4]

$$\Phi(r, \theta, \phi) = \sum_{n=0}^{\infty} \sum_{m=-n}^{n} \left(\frac{A_{nm}}{r^{n+1}} + B_{nm}r^n\right) Y_n^m(\theta, \phi). \tag{13}$$

Here, the expansion terms with coefficients A_{nm} are called a *multipole expansion*, while the terms with coefficients B_{nm} are called a *local expansion*.[4,45–48]

To solve the Poisson equation [Eqs. (3)–(6)] using the MoM, we first write the potential in the exterior region as a multipole expansion,

$$\Phi_{\text{out}}(\mathbf{r}) = \sum_{i=1}^{N} \sum_{n,m}^{p} \frac{A_{nm}^i}{r_i^{n+1}} Y_n^m(\theta_i, \phi_i), \tag{14}$$

where $\sum_{n,m}^{p}$ is short for the pth-order truncated multipole expansion summation $\sum_{n=0}^{p} \sum_{m=-n}^{n}$ and A_{nm}^i are the unknown multipole

expansion coefficients. Note that (r_i, θ_i, ϕ_i) denote the spherical coordinates of $\mathbf{r}$ with $\mathbf{o}_i$ as the origin.

Similarly, the electrostatic potential inside the ith dielectric sphere can be written as the sum of the Coulomb potential due to its own charge and the remaining polarization potential (which includes the potential due to the free charge on other spheres), which in turn can be written as a local expansion,[46]

$$
\Phi_{\text{in}}^i(\mathbf{r}) = \frac{Q_i}{4\pi\varepsilon_i|\mathbf{r} - \mathbf{o}_i|} + \sum_{n,m}^p B_{nm}^i r_i^n Y_n^m(\theta_i, \phi_i)
$$
$$
= \sum_{n,m}^p \left(B_{nm}^i r_i^n + \frac{Q_i}{4\pi\varepsilon_i r_i^{n+1}} \delta_{n0} \right) Y_n^m(\theta_i, \phi_i), \quad (15)
$$

for $i = 1, \ldots, N$, where δ_{ij} is the Kronecker delta and the coefficients B_{nm}^i are unknown. Note that here we absorb the Coulomb potential into the harmonic expansion as a monopole term.

To determine the coefficients A_{nm}^i and B_{nm}^i in Eqs. (14) and (15), we apply the interfacial conditions [Eqs. (5) and (6)]. First, we rewrite the potential in the exterior region Eq. (14) for sphere i as

$$
\Phi_{\text{out}}^i(\mathbf{r}) = \sum_{n,m}^p \left(\frac{A_{nm}^i}{r_i^{n+1}} + L_{nm}^i r_i^n \right) Y_n^m(\theta_i, \phi_i), \quad (16)
$$

where $i = 1, \ldots, N$. The new coefficients L_{nm}^i in Eq. (16) are a re-expansion for the multipole coefficients A_{nm}^j ($j \neq i$) for all other dielectric spheres in the system about the center of sphere i. If we write the coefficients for each sphere in the vector forms $\mathbf{A}^i$ and $\mathbf{B}^i$, we can define the vector $\mathbf{L}^i$ as

$$
\mathbf{L}^i = \sum_{\substack{j=1 \\ j \neq i}}^N \left(\mathcal{T}^{(i,j)} \mathbf{A}^j \right)_{nm}, \quad (17)
$$

where $\mathcal{T}^{(i,j)}$ refers to the multipole to local ("M2L") translation operator,[39,46] which transforms a multipole expansion centered at $\mathbf{o}_j$ into a local expansion centered at $\mathbf{o}_i$. The use of the $\mathcal{T}^{(i,j)}$ operator allows us to represent the potential in the exterior region due to all dielectric spheres into a unified coordinate frame of a single sphere. This is essential for solving the problem [Eq. (9)] by applying the interface conditions [Eqs. (5) and (6)] on each sphere and deriving a linear system for the multipole expansion coefficients. After substituting Eqs. (15) and (16) into the interface conditions and applying the orthogonality of spherical harmonics, we obtain the following linear system for the unknown coefficients A_{nm}^i and B_{nm}^i:

$$
\frac{A_{nm}^i}{a_i^{2n+1}} + L_{nm}^i = B_{nm}^i + C^i \delta_{n0}, \quad (18)
$$

$$
-(n+1)\frac{A_{nm}^i}{a_i^{2n+1}} + nL_{nm}^i = n\frac{\varepsilon_i}{\varepsilon_s} B_{nm}^i - (n+1)\frac{\varepsilon_i}{\varepsilon_s} C^i \delta_{n0}, \quad (19)
$$

for $n = 0, \ldots, p$; $m = -n, \ldots, n$; $i = 1, \ldots, N$. The constants C^i are defined as $C^i = Q_i/(4\pi\varepsilon_i a_i)$. We can reduce the size of this linear system by a factor two if we eliminate B_{nm}^i from Eqs. (18) and (19) and write it as a linear system only in terms of A_{nm}^i,

$$
A_{nm}^i = \Gamma_n^i \left(A_{nm}^i + \Lambda_n^i L_{nm}^i \right) + \frac{\varepsilon_i}{\varepsilon_s} \Lambda_n^i C^i \delta_{n0}, \quad (20)
$$

where

$$
\Gamma_n^i = \frac{n}{2n+1}\left(1 - \frac{\varepsilon_i}{\varepsilon_s}\right), \quad (21)
$$

$$
\Lambda_n^i = a_i^{2n+1}. \quad (22)
$$

Alternatively, Eq. (20) can be written in matrix form,

$$
\mathbf{A} = \mathbf{\Gamma} \cdot (\mathbf{I} + \mathbf{\Lambda} \cdot \mathbf{T}) \cdot \mathbf{A} + \mathbf{\Lambda} \cdot \mathbf{C}, \quad (23)
$$

where the precise matrix forms are defined in Appendix A. Once the coefficients A_{nm}^i have been obtained, the coefficients B_{nm}^i can easily be calculated by back-substitution via either Eq. (18) or (19). In practice, we solve the set of linear systems using the Generalized Minimal Residual (GMRES) algorithm.[49] In each GMRES iteration, the matrix–vector product involving the dense M2L translation matrix $\mathbf{T}$ is accelerated by a modified version of FMM (see Refs. 50 and 51 for details), achieving $\mathcal{O}(Np^3)$ scaling, i.e., linear in the number of spheres due to the FMM and cubic in the truncation order of the multipole expansion due to the spherical harmonic translation operations (detailed discussions in Ref. 50, Remark 3.1).

C. Image charge method for a general multipole

Since we aim to combine the MoM with the ICM and since in the MoM all sources are represented as multipoles, we need to formulate the ICM for a general multipole source. Specifically, we require the image-charge expression for a general multipole source outside a dielectric sphere.[42]

Consider a dielectric sphere of radius a and permittivity ε_i, centered at the origin and embedded in medium with a dielectric constant ε_s. A unit multipole source of arbitrary order l and degree k is placed at $\mathbf{c} = (0, 0, h)$ ($h > a$), producing the direct potential

$$
\Phi_{\text{source}}(\mathbf{r}) = \frac{1}{r_c^{l+1}} Y_l^k(\theta_c, \varphi_c), \quad l \geq k, \quad (24)
$$

where $(r_c, \theta_c, \varphi_c)$ are the spherical coordinates of $\mathbf{r} - \mathbf{c}$. The image potential Ψ inside and outside the dielectric sphere can be written as the superposition of potentials due to some point multipoles and line multipole densities, i.e.,

$$
\Psi_{\text{in}}(\mathbf{r}) = \frac{(1-\gamma)}{r_c^{l+1}} Y_l^k(\theta_c, \varphi_c) + \frac{\lambda\gamma}{h}\int_h^\infty \frac{(h/x)^{\lambda-l}}{r_x^{l+1}} Y_l^k(\theta_x, \varphi_x)\,dx, \quad (25)
$$

$$
\Psi_{\text{out}}(\mathbf{r}) = \sum_{j=k}^l N_{lj}^k \left[\frac{1}{r_g^{j+1}} Y_j^k(\theta_g, \varphi_g) - \frac{\lambda}{r_K}\int_0^{r_K} \frac{(r_K/x)^{1-\lambda-j}}{r_x^{j+1}} Y_j^k(\theta_x, \varphi_x)\,dx \right], \quad (26)
$$

where $\gamma = (\varepsilon_i - \varepsilon_s)/(\varepsilon_i + \varepsilon_s)$, $\lambda = \varepsilon_s/(\varepsilon_i + \varepsilon_s)$, $r_K = a^2/h$, $(r_g, \theta_g, \varphi_g)$, and $(r_x, \theta_x, \varphi_x)$ are the spherical coordinates of $\mathbf{r} - \mathbf{r}_K$ and $\mathbf{r} - \mathbf{x}$, respectively, with $\mathbf{r}_K = (r_K, 0, 0)$, $\mathbf{x} = (x, 0, 0)$. The coefficients N_{lj}^k have somewhat elaborate expressions, given in Appendix B. The total potential outside the sphere is the sum of Φ_{source} and Ψ_{out}. Note that Eqs. (25) and (26) reduce to the image potentials for the classical case of a point charge outside a dielectric sphere if the source is a monopole, i.e., $l = k = 0$. We also make two practical remarks. First, the integrals in Eqs. (25) and (26) are singular,

and we apply the Gauss–Jacobi quadrature rule to accurately evaluate these singular integrals [for the integral in Eq. (25), the change of variable $h/x = t$ should be made first], which turns the integrals into sums over discrete image point charges. Second, if the source is not located on the z-axis, one must first rotate the coordinate system to place the multipole source on the z-axis, then use the image expression to generate images, and finally rotate the source as well as the images back to the original coordinate system. Numerically, the rotation operation[52] for each close pair will require $\mathcal{O}(p^3)$ operations, where p is the truncation order for the spherical harmonics, i.e., $l \le p$.

D. The hybrid method

Having reviewed the MoM and ICM in Secs. III B and III D, we now proceed to schematically describe the hybrid method. For a given system of N dielectric spheres, we first define $\mathcal{C}_i$ as the set of all spheres that are "close" to sphere i,

$$\mathcal{C}_i = \{ j \mid |\mathbf{o}_j - \mathbf{o}_i| < \eta \cdot a_i, j \in \{1, \dots N\}, j \ne i\}, \quad (27)$$

where $\eta > 1$ is an adjustable parameter. Then, we incorporate the ICM in the MoM by generating the images for all close pairs. This implies changes in the multipole expansion coefficients A_{nm}^i in Eq. (14) and B_{nm}^i in Eq. (15),

$$A_{nm}^i \to A_{nm}^i + \sum_{j \in \mathcal{C}_i} \mathcal{I}_{ij}^{\text{out}} A_{nm}^j, \quad (28)$$

$$B_{nm}^i \to B_{nm}^i + \sum_{j \in \mathcal{C}_i} \mathcal{I}_{ij}^{\text{in}} A_{nm}^j. \quad (29)$$

Here, $\mathcal{I}_{ij}^{\text{out}} A_{nm}^j$ are the multipole expansion coefficients of the images outside dielectric sphere i due to the multipole source A_{nm}^i of sphere j, with $j \in \mathcal{C}_i$. Similarly, $\mathcal{I}_{ij}^{\text{in}} A_{nm}^j$ are the local expansion coefficients of the images inside sphere i due to all close spheres $j \in \mathcal{C}_i$. Finally, analogous to Eqs. (18) and (19), a modified linear system for the coefficients A_{nm}^i and B_{nm}^i is obtained by matching the boundary conditions. In this modified linear system, the most singular part of the geometrically induced ill-conditioning due to nearly touching spheres has been removed by analytically accounting for the effects of the first images. Therefore, the resulting linear system is much better conditioned and requires far fewer unknowns and only a very small number of GMRES iterations to achieve the prescribed accuracy.

1. Energy calculation

Upon substitution of Eq. (2) into Eq. (1), the electrostatic energy U reads

$$U = \frac{1}{2} \sum_{i=1}^N Q_i \Phi'(\mathbf{o}_i), \quad (30)$$

where the prime in the electrostatic potential indicates that the direct Coulomb potential due to the point source Q_i is omitted, i.e., self-interactions are excluded. Φ' at each source charge location $\mathbf{o}_i$ is obtained via substitution of Eq. (29) into Eq. (15),

$$\Phi'(\mathbf{o}_i) = \sum_{n,m}^p \left(B_{nm}^i + \sum_{j \in \mathcal{C}_i} \mathcal{I}_{ij}^{\text{in}} A_{nm}^j \right) r_i^n Y_n^m(\theta_i, \varphi_i) = B_{00}^i + \sum_{j \in \mathcal{C}_i} \mathcal{I}_{ij}^{\text{in}} A_{00}^j. \quad (31)$$

The second step follows from the fact that $r_i = 0$ at $\mathbf{o}_i$. As a result, the electrostatic energy can be written as

$$U = \frac{1}{2} \sum_{i=1}^N Q_i \left(B_{00}^i + \sum_{j \in \mathcal{C}_i} \mathcal{I}_{ij}^{\text{in}} A_{00}^j \right). \quad (32)$$

Physically, B_{00}^i represents the potential at the center of sphere i due to the sum of all multipole sources, whereas the second term in brackets represents the potential due to all the images generated by nearby spheres.

2. Induced surface charge density

Since variation of the dielectric constant only occurs at the spherical interfaces, the bound charge density $\rho_b(\mathbf{r})$ (cf. Sec. II) reduces to an induced *surface* charge density $\sigma_b(\mathbf{r})$. The induced surface charge density on sphere i, denoted as $\sigma_b^i(\mathbf{r})$, satisfies[4]

$$\sigma_b^i(\mathbf{r}) = \left. \frac{\partial \Phi(\mathbf{r})}{\partial r} \right|_{\mathbf{r}=\mathbf{r}^-} - \left. \frac{\partial \Phi(\mathbf{r})}{\partial r} \right|_{\mathbf{r}=\mathbf{r}^+}, \quad \mathbf{r} \in S_i. \quad (33)$$

Within the MoM, we calculate σ_b^i using the expressions Eqs. (15) and (16) for $\Phi(\mathbf{r}^-)$ and $\Phi(\mathbf{r}^+)$, respectively,

$$\sigma_b^i(\mathbf{r}) = \sum_{n,m}^p \Bigg[nB_{nm}^i a_i^{n-1} - \frac{Q_i}{4\pi\varepsilon_i a_i^2} \delta_{n0}$$
$$+ (n+1) \frac{A_{nm}^i}{a_i^{n+2}} - nL_{nm}^i a_i^{n-1} \Bigg] Y_n^m(\theta_i, \phi_i), \quad \mathbf{r} \in S_i, \quad (34)$$

with $\mathbf{r} = (a_i, \theta_i, \phi_i)$. This can be simplified further by eliminating B_{nm}^i using Eq. (18),

$$\sigma_b^i(\mathbf{r}) = \sum_{n,m}^p \left[(2n+1) \frac{A_{nm}^i}{a_i^{n+2}} - \frac{Q_i}{4\pi\varepsilon_i a_i^2} \delta_{n0} \right] Y_n^m(\theta_i, \phi_i). \quad (35)$$

The induced surface charge density thus obtained can be used to calculate the potential or field at any point in space as if there were no dielectric interfaces, according to Eq. (10). Although these expressions only apply to the MoM, they can directly be extended to the hybrid method by simply making the substitutions in Eqs. (28) and (29) for A_{nm}^i and B_{nm}^i, respectively, to account for the image multipoles for close pairs of spheres.

3. Force calculation

The evolution of MD and Brownian dynamics simulations requires the force on each dielectric sphere. In addition, forces are useful for the calculation of pressure in both dynamic and MC simulations. Note that, since the free charge is located at the center of each sphere and the induced charge does not rotate rigidly with the object, it is not necessary to include torques in the model. The total force $\mathbf{F}^i$ exerted on dielectric sphere i is[26]

$$\mathbf{F}^i = \int_{S_i} \varepsilon_s (\sigma_f^i + \sigma_b^i) \mathbf{E} \, dS, \quad (36)$$

where $\sigma_f^i = Q_i / (4\pi\varepsilon_i a_i^2)$ is the free surface charge density equivalent to the central charge Q_i and $\mathbf{E}(\mathbf{r})$ for $\mathbf{r}$ located on the sphere surface is defined as

$$\mathbf{E}(\mathbf{r}) = -\frac{1}{2}\nabla\left[\Phi(\mathbf{r}^-) + \Phi(\mathbf{r}^+)\right] \quad \mathbf{r} \in S_i. \tag{37}$$

Equation (37) is only valid if the interface is smooth, as proven rigorously in Ref. 53, Theorem 6.18. For cases with a nonsmooth boundary, such as the electric field at a corner point, Eq. (37) needs to be modified (cf. Ref. 53, Sec. 6.5). Substituting Eqs. (35) and (37) into Eq. (36), we obtain the force exerted on sphere i,

$$\mathbf{F}^i = \int_{S_i} -\sum_{n,m}^{p}\left(n + \frac{1}{2}\right)\frac{A_{nm}^i}{a_i^{n+2}}Y_n^m(\theta_i,\phi_i)\nabla\left[\Phi(\mathbf{r}^-) + \Phi(\mathbf{r}^+)\right]d\mathbf{r}. \tag{38}$$

The potentials $\Phi(\mathbf{r}^-)$ and $\Phi(\mathbf{r}^+)$ are also expressed in terms of spherical harmonics via Eqs. (15) and (16) so that the gradients can be calculated analytically. In the hybrid method, the coefficients A_{nm}^i and B_{nm}^i in these potentials [including the coefficients L_{nm}^i in Eq. (16), which depend on A_{nm}^i via Eq. (17)], and also in Eq. (38), must be substituted according to Eqs. (28) and (29).

Obtaining the coefficients A_{nm}^i, B_{nm}^i, and L_{nm}^i involves a computational cost $\mathcal{O}(N)$ for N spheres. Since the force on each sphere is represented as an integral over the sphere, the cost of obtaining all forces therefore also scales linearly with the number of spheres. In practice, the surface integral is accurately evaluated by constructing a set of quadrature nodes and weights on each sphere (Gauss–Legendre nodes along the θ direction and equispaced nodes along the ϕ direction, as described in Ref. 42, Sec. 4.4, Algorithm 1).

IV. NUMERICAL TESTS: STATIC CONFIGURATIONS

To illustrate the accuracy and efficiency of the hybrid method, we apply it to representative close-packed crystal structures formed by a binary mixture of size-asymmetric and oppositely charged dielectric spheres. We examine two crystal structures, namely, a NaCl and a wurtzite structure, illustrated in Fig. 1. Such densely packed structures with closely spaced dielectric interfaces are generally challenging for most numerical methods. Disordered configurations occurring in dynamic simulations tend to have fewer of the particle arrangements that yield the largest numerical errors and are typically also less costly to evaluate as the number of image charges needed is generally smaller. The large and small spheres have
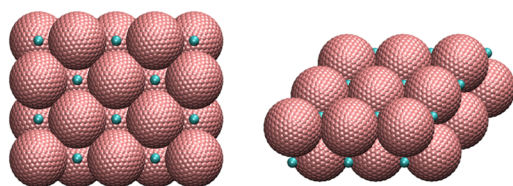

FIG. 1. Two crystal structures formed by binary size-asymmetric dielectric spheres, used for testing the hybrid method. (Left) NaCl crystal structure with lattice constant $\sqrt{2}d_L$ formed by 20 large spheres and 20 small spheres; (right) wurtzite crystal structure with lattice constants $a = b = d_L$, $c = 2\sqrt{2}d_L/\sqrt{3}$, formed by 18 large spheres and 18 small spheres. The lattice constants are chosen such that the large spheres are precisely touching. Since the dielectric interface is located $0.5d_s$ below the sphere surface, the dielectric surfaces of two touching spheres are separated by d_s.

diameters d_L and d_s, respectively, and a size ratio $d_L/d_s = 8$. To avoid divergences due to the overlap of two dielectric interfaces, we place the dielectric surface of each large sphere at $r = 3.5d_s$, i.e., $0.5d_s$ below the sphere surface. The large spheres each carry a charge $+q$, and the small spheres each carry a charge $-q$. The two species are present in a 1:1 number ratio so that charge neutrality is satisfied. We select interaction parameters similar to those chosen in Ref. 9, where the dielectric constant of the solvent is rescaled to $\varepsilon_s = 1.0$ and the small spheres have the same dielectric constant as the solvent. For the NaCl structure, we set the dielectric constant of the large spheres to $\varepsilon_L = 0.01$, whereas for the wurtzite structure we choose the inverse mismatch, with $\varepsilon_L = 100$. In both cases, the magnitude of the charge q is chosen such that the dimensionless coupling strength $q^2/[0.5\varepsilon_s(d_L + d_s)k_B T] = 100$, where $k_B T$ is the thermal energy (with k_B as Boltzmann's constant and T as the absolute temperature).

To obtain reference values for these two static configurations, we first calculate the energy for both structures using the analytic MoM. The multipole expansion is truncated at a sufficiently high order ($p = 30$) to guarantee that the energies are correct to the first six digits, with values $-1028.49 k_B T$ and $-2267.41 k_B T$ for the NaCl and wurtzite configurations, respectively. To quantify the performance of the hybrid method, we compute both the total electrostatic energy of the configurations and the net electrostatic force exerted on each sphere. We examine the convergence of the hybrid method as a function of algorithm parameters by comparison to the corresponding reference values. To establish the efficiency of the hybrid method, we also compute the results via the BEM of Ref. 26.

In the hybrid method, we set the FMM accuracy to 9 digits and the GMRES tolerance to 10^{-6} and use 3-point Gauss–Jacobi quadrature for discretizing the image line integrals in Eqs. (25) and (26). The accuracy of the hybrid method is then solely determined by the truncation order p for the spherical harmonics and the number of image charges [via η in Eq. (27)]. Table I lists the energies for both systems as a function of these two parameters.

As we systematically increase p and η, we observe a clear convergence of the energy for both the NaCl and wurtzite structures (left-hand side of Table I). Specifically, in both cases, the energy is accurate up to the fifth digit at $p = 5$ and $\eta = 6$, with a moderate number of image charges (~130 image charges per sphere). As the computational cost of the hybrid method is proportional to both p^3 and η^3, we gradually increase both parameters simultaneously in Table I to keep both of them sufficiently small.

For the BEM, the accuracy is controlled by the accuracy of the particle–particle particle–mesh (PPPM) electrostatic solver, the GMRES tolerance, and the number of surface patches. By testing different combinations of the PPPM and GMRES accuracies, we empirically determined that (at fixed number of patches) the energy converges to at least the fourth digit if both are set to 10^{-5}. We employ these tolerances for all BEM data shown and only vary the number of surface elements. It should be noted that the BEM calculations are performed for a system with periodic boundary conditions so that the system size matters. We used a cube of linear size $L = 60d_s$ and confirmed (by comparison to $L = 100d_s$ and $L = 200d_s$) that this periodicity has an effect of less than 10^{-4} on the energy. We systematically vary the number of patches on

TABLE I. Accuracy and efficiency of the hybrid method and the BEM for the electrostatic energy calculation of the NaCl and wurtzite configurations in Fig. 1. All CPU time results are obtained by averaging over 100 calculations of both the total energy and the force on each large dielectric spheres (the initialization time is not counted in both methods). For both methods, the corresponding numerical parameters are varied to show the convergence (as reference values we use the energies computed via the analytic MoM at $p = 30$, $-1028.49 k_B T$ for the NaCl configuration and $-2267.41 k_B T$ for the wurtzite configuration). p is the order at which the multipole expansion is truncated in the hybrid method, and η is the cutoff that controls the total number of images N_{im} between close pairs. In the BEM, N_p is the number of the discretized patches on each large sphere. The results with $N_p \rightarrow \infty$ are obtained by extrapolation, cf. Fig. 2. Timing data for the BEM data with $N_p = 14\,522$ are affected by memory constraints and therefore not reported.

	Hybrid method					Boundary element method		
	p	η	N_{im}	Energy ($k_B T$)	Time (s)	N_p	Energy ($k_B T$)	Time (s)
NaCl crystal	3	3	480	−1009.20	0.014	372	−1098.86	1.116
	3	4	1392	−1038.23	0.047	732	−1077.85	1.355
	4	4	1392	−1023.76	0.056	1 472	−1062.54	2.284
	4	5	1614	−1023.73	0.069	3 002	−1051.56	6.320
	5	5	1614	−1028.38	0.084	6 072	−1043.88	21.341
	5	6	2688	−1028.43	0.140	14 522	−1037.55	n/a
						∞	−1025.80	
Reference				−1028.49			−1028.49	
Wurtzite crystal	3	3	508	−2375.67	0.014	372	−2326.40	1.112
	3	4	1194	−2382.37	0.037	732	−2310.07	1.335
	4	4	1194	−2284.24	0.044	1 472	−2297.53	2.215
	4	5	1518	−2282.63	0.061	3 002	−2288.63	5.812
	5	5	1518	−2272.37	0.074	6 072	−2282.39	19.772
	5	6	2216	−2267.43	0.081	14 522	−2277.17	n/a
						∞	−2267.90	
Reference				−2267.41			−2267.41	

each large sphere N_p from 372 to 14 522 and compute the total electrostatic energy of both configurations (right-hand side of Table I). The energy values show a quite strong dependence on N_p, but a plot of the energy as a function of $1/\sqrt{N_p}$ (which is proportional to the boundary element size), Fig. 2, illustrates convergence to −1025.80 for the NaCl structure and −2267.90 for the wurtzite structure as $N_p \rightarrow \infty$. These values are in quite good agreement with the reference values, deviating by 0.3% and 0.03%, respectively. The linear convergence with boundary-element size has been reported for other BEM approaches.[54,55] Whereas a fairly accurate estimate for the energy can be obtained in the BEM through extrapolation, this is not a particularly useful approach in a practical MD or MC simulation, where each run employs only a single number of surface patches. Without the extrapolation, the BEM shows deviations of ~1% even at the largest N_p (14 522 patches per large sphere) tested here, owing to the closely separated dielectric interfaces.

Since MD simulations evolve via Newton's equations of motion, i.e., based upon forces rather than energies, we also compare the force exerted on each sphere in the hybrid method and the BEM. Since these forces are not extrapolated as a function of N_p in an actual (BEM-based) MD simulation, we directly compare the

forces obtained in the BEM at $N_p = 14\,522$ with those obtained in the hybrid method at $p = 5$ and $\eta = 6$. The relative root-mean-square difference in the forces is defined as

$$\Delta_F = \sqrt{\frac{\sum_{i=1}^{N} |\mathbf{F}_{HM}^i - \mathbf{F}_{BEM}^i|^2}{\sum_{i=1}^{N} |\mathbf{F}_{HM}^i|^2}}, \quad (39)$$

where the summation extends over all large spheres, and $\mathbf{F}_{HM}^i$ and $\mathbf{F}_{BEM}^i$ denote the electrostatic force exerted on sphere i computed via the hybrid method and the BEM, respectively. We find that the relative discrepancy Δ_F is 0.6% and 2.6% for the NaCl and wurtzite crystal test cases, respectively.

The hybrid method needs far fewer image charges than the number of patches in the BEM to achieve a high accuracy. Since the electrostatic solver is the dominant factor in the computational cost of the induced energy and force calculation, the hybrid method accordingly outperforms the BEM (see the CPU time comparison in Table I). At four-digit accuracy in the electrostatic energy, the hybrid method (with $p = 5$, $\eta = 6$) is more than a 100 times faster than the BEM for $N_p = 6072$ (which yields significantly lower accuracy) for both test cases.
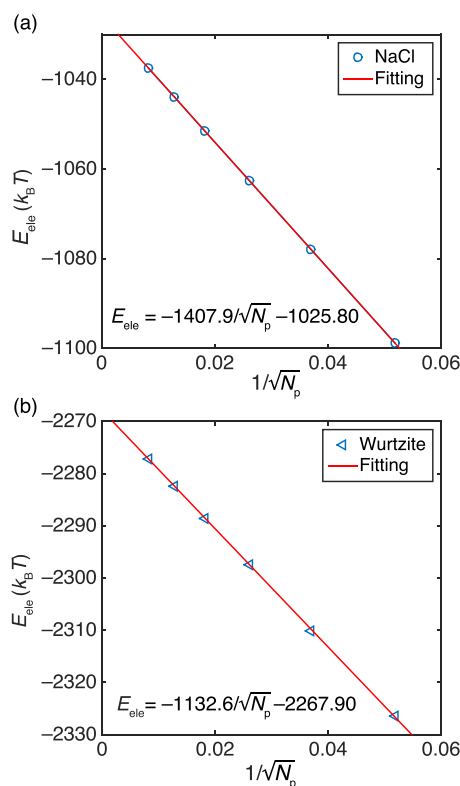
FIG. 2. Extrapolation of the electrostatic energy E_{ele} in the BEM as a function of $1/\sqrt{N_p}$ (N_p being the number of surface patches per sphere) for the (a) NaCl and (b) wurtzite crystal structures. The extrapolated values are in close agreement with the reference values obtained via the method of moments.

V. MD SIMULATIONS: ENSEMBLE AVERAGES

Whereas numerical tests on static configurations provide information on accuracy and on the appropriate numerical parameter settings, it is also informative to apply the hybrid method to practical simulations of the aggregation of a binary mixture of dielectric spheres. We examine the performance of the method and also cross-check ensemble-averaged equilibrium properties with simulations performed using the BEM.

We employ the same parameter settings as the NaCl case tested in Sec. IV. In addition to the electrostatic interactions, we impose excluded-volume interactions modeled via a shift-truncated Lennard-Jones (LJ) potential,

$$u_{LJ}(r) = 4k_B T\left[\left(\frac{d_s}{r-\Delta}\right)^{12} - \left(\frac{d_s}{r-\Delta}\right)^6 + \frac{1}{4}\right], \quad (40)$$

for $\Delta < r \leq 2^{\frac{1}{6}}d_s + \Delta$, with $\Delta = 0$, $3.5d_s$, and $7d_s$ for small–small, small–large, and large–large interactions, respectively. This yields a large–small size ratio of 8. As before, we place the dielectric surface of each large sphere at $r = 3.5d_s$, where the purely repulsive LJ potential already diverges. The mass of all spheres, which affects the dynamical evolution of the system but not its thermodynamic properties, is set to m_0, yielding a time scale $t_0 = d_s\sqrt{m_0/k_B T}$.

We perform MD simulations of a binary mixture containing 20 large and 20 small spheres. For the hybrid method, the system is confined in a spherical cell with cell radius $R_{shell} = 30d_s$ and the algorithm parameters are set to $p = 5$ and $\eta = 6$. For the BEM, we employ a cubic cell of size $L = 60d_s$ and periodic boundary conditions. The number of patches per large sphere is set to $N_p = 1472$, for reasons of computational feasibility. The tolerances are set as detailed in Sec. IV.

In each time step, the (direct and induced) electrostatic force on each particle is calculated and used to propagate the particles via the standard velocity-Verlet algorithm. A Langevin thermostat with damping time t_0 is used to control the temperature. Simulations are run for 5×10^5 steps for equilibration and another 5×10^5 steps to generate samples, with a time step of $0.001t_0$. The various contributions to the total energy as well as the radial distribution functions are sampled every 500 steps during the production phase.

The equilibrated structure is predicted to be a NaCl crystal,[9] which is confirmed visually for both methods. Moreover, the radial distribution function for the large spheres (Fig. 3) produced by the hybrid method is almost identical to that produced by the
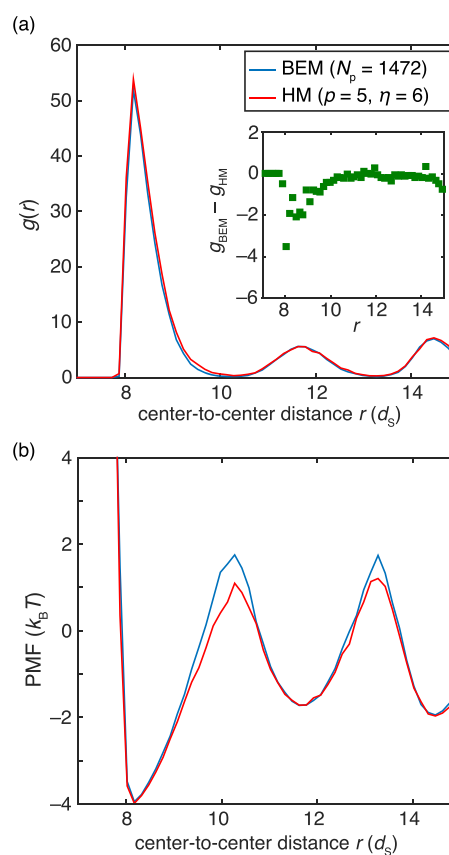

FIG. 3. (a) Large–large particle radial distribution function for the system described in Sec. V, obtained using the BEM (blue curve) and the hybrid method (HM, red curve). Inset: difference between the two distribution functions. (b) Corresponding potential of mean force $-k_B T \ln g(r)$.

TABLE II. Ensemble averaged electrostatic and LJ energies obtained through MD simulations using the hybrid method and BEM.

Numerical parameters	E_{ele}	E_{LJ}
Hybrid method		
$p = 4, \eta = 4$	-954.0 ± 0.5	3.58 ± 0.07
$p = 4, \eta = 5$	-941.4 ± 0.6	2.69 ± 0.06
$p = 5, \eta = 6$	-943.9 ± 0.6	2.69 ± 0.05
Boundary element method		
$N_p = 372$	-1019.3 ± 0.8	2.98 ± 0.06
$N_p = 732$	-997.5 ± 0.9	2.86 ± 0.06
$N_p = 1472$	-984.5 ± 0.8	3.00 ± 0.06

BEM-based simulation. While the two dielectric solvers show excellent consistency in the self-assembled structure, the hybrid method achieves this at a rate of 0.140 s per time step, compared to 2.284 s per time step for the BEM (see Table I). In addition, the static tests show that for the settings adopted, the hybrid method yields an electrostatic energy that is virtually indistinguishable from the reference value, whereas the BEM yields an energy that deviates from this value by more than 3%. As this deviation refers to a truly dense-packed configuration, it is worthwhile to examine whether the ensemble-averaged energy shows a similar deviation. Table II shows the ensemble-averaged energies for MD simulations employing either the hybrid method or the BEM, with different parameter settings. Even though the hybrid and BEM simulations with the most precise parameter choices produced very similar self-assembled structures, the average electrostatic energies differ by approximately 4%, comparable to the difference in Table I for the same parameters.

VI. SUMMARY

We have extended the recently introduced hybrid electrostatic solver to calculate direct and induced electrostatic forces between dielectric spheres and have incorporated this approach in a molecular dynamics simulation. Unlike boundary-element approaches, which suffer from significant inaccuracies in situations with closely spaced dielectric interfaces (such as in densely packed structures), and other analytical approaches, which require an effort that increases rapidly (at least cubic power-law dependence) with the number of dielectric spheres, the hybrid solver simultaneously offers linear scaling behavior and high accuracy.

We have provided a concise review of the hybrid method, systematically explored the effect of various parameters on efficiency, convergence, and accuracy, and illustrated application of the method in a practical case that is challenging for competing approaches. We demonstrated that, for densely packed configurations of relatively small numbers of dielectric spheres, the hybrid method computes the electrostatic energy with a deviation of less than 0.01% at a rate that is more than two orders of magnitude faster than the BEM can achieve for deviations of 3%.

This approach is generally applicable to multicomponent systems of charged dielectric spheres. In principle, extension of our method to continuously variable, radially symmetric permittivities $\varepsilon(r)$ is feasible by using a harmonic interpolation,[56] which results in a spherical harmonic series than can be transformed into an image-charge method. Finally, although the current algorithm is restricted to finite systems, we plan to extend it to situations with periodic boundary conditions.

APPENDIX A: MATRICES FOR THE LINEAR SYSTEM OBTAINED IN THE METHOD OF MOMENTS

The matrices in the linear system in Eq. (23) are given by

$$\mathbf{A} = \begin{pmatrix} \mathbf{A}^1 \\ \mathbf{A}^2 \\ \vdots \\ \mathbf{A}^N \end{pmatrix}, \quad \mathbf{\Gamma} = \begin{pmatrix} \mathbf{\Gamma}^1 & 0 & \cdots & 0 \\ 0 & \mathbf{\Gamma}^2 & \ddots & \vdots \\ \vdots & \ddots & \ddots & 0 \\ 0 & \cdots & 0 & \mathbf{\Gamma}^N \end{pmatrix}, \quad \mathbf{\Lambda} = \begin{pmatrix} \mathbf{\Lambda}^1 & 0 & \cdots & 0 \\ 0 & \mathbf{\Lambda}^2 & \ddots & \vdots \\ \vdots & \ddots & \ddots & 0 \\ 0 & \cdots & 0 & \mathbf{\Lambda}^N \end{pmatrix},$$

$$(A1)$$

$$\mathbf{T} = \begin{pmatrix} 0 & \mathcal{T}^{(1,2)} & \cdots & \mathcal{T}^{(1,N)} \\ \mathcal{T}^{(2,1)} & 0 & \ddots & \vdots \\ \vdots & \ddots & \ddots & \mathcal{T}^{(N-1,N)} \\ \mathcal{T}^{(N,1)} & \cdots & \mathcal{T}^{(N,N-1)} & 0 \end{pmatrix}, \quad \mathbf{C} = \begin{pmatrix} \mathbf{C}^1 \\ \mathbf{C}^2 \\ \vdots \\ \mathbf{C}^N \end{pmatrix},$$

$$(A2)$$

and

$$\mathbf{\Gamma}^i = \begin{pmatrix} \Gamma_0^i & 0 & \cdots & 0 \\ 0 & \Gamma_1^i & \ddots & \vdots \\ \vdots & \ddots & \ddots & 0 \\ 0 & \cdots & 0 & \Gamma_p^i \end{pmatrix}, \quad \mathbf{\Lambda}^i = \begin{pmatrix} \Lambda_0^i & 0 & \cdots & 0 \\ 0 & \Lambda_1^i & \ddots & \vdots \\ \vdots & \ddots & \ddots & 0 \\ 0 & \cdots & 0 & \Lambda_p^i \end{pmatrix},$$

$$(A3)$$

$$\mathbf{C}^i = \begin{pmatrix} \frac{\varepsilon_i}{\varepsilon_s} C^i & 0 & \cdots & 0 \\ 0 & 0 & \ddots & \vdots \\ \vdots & \ddots & \ddots & 0 \\ 0 & \cdots & 0 & 0 \end{pmatrix}.$$

APPENDIX B: COEFFICIENTS FOR THE MULTIPOLE IMAGE CHARGE FORMULA

The coefficients N_{lj}^k ($j = k, \ldots, l$) in the image-charge expression equation (26) are given by

$$
\begin{cases}
N_{lk}^k = (-1)^{l+1} \gamma \dfrac{(l+k)!}{(2k)!} \dfrac{a^{2k+1}}{h^{l+k+1}} G_l^k, \\[2ex]
N_{lj}^k = (-1)^{l+1} \gamma \dfrac{a^{2j+1}}{h^{l+j+1}} \sqrt{\dfrac{(j+k)!(j-k)!}{(2k)!}} G_l^k \\[2ex]
\qquad \times \displaystyle\sum_{i=j-k}^{l-k} \dfrac{(l+k-i)!(i-j+k)!}{(2k)!} \binom{l-k}{i}\binom{i}{j-k}\binom{i-1}{j-k-1}, \qquad j = k+1, \ldots, l,
\end{cases}
\tag{B1}
$$

where

$$
G_l^k = \sqrt{\dfrac{(2k)!}{(l+k)!(l-k)!}}
\tag{B2}
$$

and the parameters a and h are defined in Sec. III C.

An alternative recurrence relation that permits calculation of N_{lj}^k is

$$
\begin{cases}
N_{lk}^k = (-1)^{l+1} \gamma \sqrt{\dbinom{l+k}{l-k}} \dfrac{a^{2k+1}}{h^{l+k+1}} G_l^k, \\[2ex]
N_{lj}^k = (-1)^{l+1} \gamma \sqrt{\dbinom{l+j}{l+k}\dbinom{l+j}{l-k}} \dfrac{a^{2j+1}}{h^{l+j+1}} G_l^k \\[2ex]
\qquad - \displaystyle\sum_{i=1}^{j-k} N_{j-i}^k \sqrt{\dbinom{j+k}{i}\dbinom{j-k}{i}} \left(\dfrac{a^2}{h}\right)^i, \quad j = k+1, \ldots, l.
\end{cases}
\tag{B3}
$$

REFERENCES

[1] B. Honig and A. Nicholls, "Classical electrostatics in biology and chemistry," Science **268**, 1144–1149 (1995).

[2] R. H. French, V. A. Parsegian, R. Podgornik, R. F. Rajter, A. Jagota, J. Luo, D. Asthagiri, M. K. Chaudhury, Y.-m. Chiang, S. Granick, S. Kalinin, M. Kardar, R. Kjellander, D. C. Langreth, J. Lewis, S. Lustig, D. Wesolowski, J. S. Wettlaufer, W.-Y. Ching, M. Finnis, F. Houlihan, O. A. von Lilienfeld, C. J. van Oss, and T. Zemb, "Long range interactions in nanoscale science," Rev. Mod. Phys. **82**, 1887–1944 (2010).

[3] D. A. Walker, B. Kowalczyk, M. Olvera de la Cruz, and B. A. Grzybowski, "Electrostatics at the nanoscale," Nanoscale **3**, 1316–1344 (2011).

[4] J. D. Jackson, *Classical Electrodynamics*, 3rd ed. (Wiley, New York, 1999).

[5] A. Zangwill, *Modern Electrodynamics* (Cambridge University Press, Cambridge, UK, 2013).

[6] A. van der Vaart, B. D. Bursulaya, C. L. Brooks III, and K. M. Merz, "Are many-body effects important in protein folding?," J. Phys. Chem. B **104**, 9554–9563 (2000).

[7] R. Allen, S. Melchionna, and J.-P. Hansen, "Intermittent permeation of cylindrical nanopores by water," Phys. Rev. Lett. **89**, 175502 (2002).

[8] H. S. Antila and E. Luijten, "Dielectric modulation of ion transport near interfaces," Phys. Rev. Lett. **120**, 135501 (2018).

[9] K. Barros and E. Luijten, "Dielectric effects in the self-assembly of binary colloidal aggregates," Phys. Rev. Lett. **113**, 017801 (2014).

[10] C. A. Silvera Batista, R. G. Larson, and N. A. Kotov, "Nonadditivity of nanoparticle interactions," Science **350**, 1242477 (2015).

[11] D. G. Levitt, "Electrostatic calculations for an ion channel. I. Energy and potential profiles and interactions between ions," Biophys. J. **22**, 209–219 (1978).

[12] R. J. Zauhar and R. S. Morgan, "A new method for computing the macromolecular electric potential," J. Mol. Biol. **186**, 815–820 (1985).

[13] H. Hoshi, M. Sakurai, Y. Inoue, and R. Chûjô, "Medium effects on the molecular electronic structure. I. The formulation of a theory for the estimation of a molecular electronic structure surrounded by an anisotropic medium," J. Chem. Phys. **87**, 1107–1115 (1987).

[14] A. H. Juffer, E. F. F. Botta, B. A. M. van Keulen, A. van der Ploeg, and H. J. C. Berendsen, "The electric potential of a macromolecule in a solvent: A fundamental approach," J. Comput. Phys. **97**, 144–171 (1991).

[15] A. Nicholls and B. Honig, "A rapid finite difference algorithm, utilizing successive over-relaxation to solve the Poisson–Boltzmann equation," J. Comput. Chem. **12**, 435–445 (1991).

[16] N. A. Baker, D. Sept, S. Joseph, M. J. Holst, and J. A. McCammon, "Electrostatics of nanosystems: Application to microtubules and the ribosome," Proc. Natl. Acad. Sci. U. S. A. **98**, 10037–10041 (2001).

[17] R. Allen, J.-P. Hansen, and S. Melchionna, "Electrostatic potential inside ionic solutions confined by dielectrics: A variational approach," Phys. Chem. Chem. Phys. **3**, 4177–4186 (2001).

[18] A. C. Maggs and V. Rossetto, "Local simulation algorithms for Coulomb interactions," Phys. Rev. Lett. **88**, 196402 (2002).

[19] D. Boda, D. Gillespie, W. Nonner, D. Henderson, and B. Eisenberg, "Computing induced charges in inhomogeneous dielectric media: Application in a Monte Carlo simulation of complex ionic systems," Phys. Rev. E **69**, 046702 (2004).

[20] J. Rottler and A. C. Maggs, "Local molecular dynamics with Coulombic interactions," Phys. Rev. Lett. **93**, 170201 (2004).

[21] I. Pasichnyk and B. Dünweg, "Coulomb interactions via local dynamics: A molecular-dynamics algorithm," J. Phys.: Condens. Matter **16**, S3999–S4020 (2004).

[22] P.-G. Martinsson, "Fast evaluation of electro-static interactions in multi-phase dielectric media," J. Comput. Phys. **211**, 289–299 (2006).

[23] S. Tyagi, M. Süzen, M. Sega, M. Barbosa, S. S. Kantorovich, and C. Holm, "An iterative, fast, linear-scaling method for computing induced charges on arbitrary dielectric boundaries," J. Chem. Phys. **132**, 154112 (2010).

[24] R. Yokota, J. P. Bardhan, M. G. Knepley, L. A. Barba, and T. Hamada, "Biomolecular electrostatics using a fast multipole BEM on up to 512 gpus and a billion unknowns," Comput. Phys. Commun. **182**, 1272–1283 (2011).

[25] V. Jadhao, F. J. Solis, and M. Olvera de la Cruz, "Simulation of charged systems in heterogeneous dielectric media via a true energy functional," Phys. Rev. Lett. **109**, 223905 (2012).

[26] K. Barros, D. Sinkovits, and E. Luijten, "Efficient and accurate simulation of dynamic dielectric objects," J. Chem. Phys. **140**, 064903 (2014).

[27] H. Wu and E. Luijten, "Accurate and efficient numerical simulation of dielectrically anisotropic particles," J. Chem. Phys. **149**, 134105 (2018).

[28] D. R. McKenzie, R. C. McPhedran, and G. H. Derrick, "The conductivity of lattices of spheres. II. The body centred and face centred cubic lattices," Proc. R. Soc. A **362**, 211–232 (1978).

[29] R. C. McPhedran and D. R. McKenzie, "The conductivity of lattices of spheres. I. The simple cubic lattice," Proc. R. Soc. A **359**, 45–63 (1978).

[30] A. S. Sangani and A. Acrivos, "The effective conductivity of a periodic array of spheres," Proc. R. Soc. A **386**, 263–275 (1983).

[31] K. Hinsen and B. U. Felderhof, "Dielectric constant of a suspension of uniform spheres," Phys. Rev. B **46**, 12955–12963 (1992).

[32] L. Greengard and M. Moura, "On the numerical evaluation of electrostatic fields in composite materials," Acta Numer. **3**, 379–410 (1994).

[33] W. Thomson, "Extrait d'une lettre de M. William Thomson à M. Liouville," J. Math. Pure Appl. **10**, 364–367 (1845).

[34] W. Thomson, "Geometrical investigations with reference to the distribution of electricity on spherical conductors," Camb. Dublin Math. J. **3**, 141–148 (1848).

[35] C. Neumann, *Hydrodynamische Untersuchungen, nebst einem Anhange über die Probleme der Elektrostatik und der Magnetischen Induction* (B. G. Teubner, Leipzig, 1883).

[36] K. F. Freed, "Perturbative many-body expansion for electrostatic energy and field for system of polarizable charged spherical ions in a dielectric medium," J. Chem. Phys. **141**, 034115 (2014).

[37] J. Qin, J. J. de Pablo, and K. F. Freed, "Image method for induced surface charge from many-body system of dielectric spheres," J. Chem. Phys. **145**, 124903 (2016).

[38] L. Greengard and V. Rokhlin, "A fast algorithm for particle simulations," J. Comput. Phys. **73**, 325–348 (1987).

[39] H. Cheng, L. Greengard, and V. Rokhlin, "A fast adaptive multipole algorithm in three dimensions," J. Comput. Phys. **155**, 468–498 (1999).

[40] L. Ying, G. Biros, and D. Zorin, "A kernel-independent adaptive fast multipole algorithm in two and three dimensions," J. Comput. Phys. **196**, 591–626 (2004).

[41] Z. Gan, H. Wu, K. Barros, Z. Xu, and E. Luijten, "Comparison of efficient techniques for the simulation of dielectric objects in electrolytes," J. Comput. Phys. **291**, 317–333 (2015).

[42] Z. Gan, S. Jiang, E. Luijten, and Z. Xu, "A hybrid method for systems of closely spaced dielectric spheres and ions," SIAM J. Sci. Comput. **38**, B375–B395 (2016).

[43] L. D. Landau, E. M. Lifshitz, and L. P. Pitaevskii, *Electrodynamics of Continuous Media*, Course of Theoretical Physics Vol. 8, 2nd ed. (Elsevier Butterworth Heinemann, Oxford, 1993).

[44] G. B. Arfken and H. J. Weber, *Mathematical Methods for Physicists*, 4th ed. (Academic Press, Boston, 1995).

[45] R. J. A. Tough and A. J. Stone, "Properties of the regular and irregular solid harmonics," J. Phys. A: Math. Gen. **10**, 1261–1269 (1977).

[46] L. Greengard, *The Rapid Evaluation of Potential Fields in Particle Systems* (The MIT Press, Cambridge, MA, 1988).

[47] O. D. Kellogg, *Foundations of Potential Theory* (Dover, New York, 1953).

[48] P. R. Wallace, *Mathematical Analysis of Physical Problems* (Dover, New York, 1984).

[49] Y. Saad and M. H. Schultz, "GMRES: A generalized minimal residual algorithm for solving nonsymmetric linear systems," SIAM J. Sci. Stat. Comput. **7**, 856–869 (1986).

[50] Z. Gimbutas and L. Greengard, "Fast multi-particle scattering: A hybrid solver for the Maxwell equations in microstructured materials," J. Comput. Phys. **232**, 22–32 (2013).

[51] A. J. Hesford, J. P. Astheimer, L. F. Greengard, and R. C. Waag, "A mesh-free approach to acoustic scattering from multiple spheres nested inside a large sphere by using diagonal translation operators," J. Acoust. Soc. Am. **127**, 850–861 (2010).

[52] L. C. Biedenharn and J. D. Louck, *Angular Momentum in Quantum Physics: Theory and Application* (Addison-Wesley, Reading, MA, 1981).

[53] R. Kress, *Linear Integral Equations*, 3rd ed. (Springer, New York, 2014).

[54] B. Lu, X. Cheng, and J. A. McCammon, "'New-version-fast-multipole-method' accelerated electrostatic calculations in biomolecular systems," J. Comput. Phys. **226**, 1348–1366 (2007).

[55] W. Geng and R. Krasny, "A treecode-accelerated boundary integral Poisson–Boltzmann solver for electrostatics of solvated biomolecules," J. Comput. Phys. **247**, 62–78 (2013).

[56] F. Fahrenberger, Z. Xu, and C. Holm, "Simulation of electric double layers around charged colloids in aqueous solution of variable permittivity," J. Chem. Phys. **141**, 064902 (2014).